Analysis of wave number spectra through the terrestrial bow shock

Y. Narita,[1] K.-H. Glassmeier,[1] S. P. Gary,[2] M. L. Goldstein,[3] and R. A. Treumann[4]

Yasuhito Narita, Institute of Geophysics and Extraterrestrial Physics, Technical University of Braunschweig, Mendelssohnstr. 3, D-38106 Braunschweig, Germany. (y.narita@tu-bs.de)

[1]Institute of Geophysics and Extraterrestrial Physics, Technical University of Braunschweig, Mendelssohnstr. 3, D-38106 Braunschweig, Germany.

[2]Los Alamos National Laboratory, Los Alamos, NM 87545, USA

[3]NASA Goddard Space Flight Center, Code 673, Greenbelt, MD 20771, USA.

[4]Department of Geoscience, Geophysics Section, Ludwig-Maximilians-University Munich, Theresienstr. 41, D-80333 Munich, Germany.

Abstract. Evolution of the magnetic field fluctuations of the solar wind across the Earth's bow shock is studied. Using the four Cluster spacecraft the energy spectra of the magnetic field fluctuations are decomposed into three distinct components in the wave number domain: two-dimensional component, Alfvénic component, and compressible component. The spectral decomposition provides a means to study how the shock-turbulence interaction occurs in the collisionless plasma. The two-dimensional component is a major contributor in the fluctuation energy throughout from the solar wind to the foreshock, the magnetosheath, and the cusp region. The solar wind exhibits the dominance of the two-dimensional component and its wave number spectrum is characterized by a power law with the index close to -5/3. The transition of the solar wind across the shock is characterized not only by amplification of the fluctuations but also by reconfiguration of the energy contributions of the three components. The foreshock and the magnetosheath exhibit enhancements of the Alfvénic and the compressible components, respectively. The reconfiguration of the energy contribution can be interpreted in such a way that the solar wind turbulence is modified by the waves that are locally excited by the shock-reflected ions or directly by the shock.

1. Introduction

Shock waves in space such as supernovae, interstellar and interplanetary shocks, and planetary bow shocks are often associated with a turbulent medium. One of the direct consequences of the shock-turbulence interaction is the acceleration of cosmic ray particles [Fermi, 1949]. How turbulence evolves as it encounters the shock wave in the collisionless medium is an interesting problem and of practical importance in space- and astrophysics. Theoretical treatments of the shock-turbulence interaction remains still as a challenge for several reasons. One of the difficulties is that the equations governing the motion of the flow velocity and the magnetic field must be solved under the condition that the turbulent field undergoes a shock wave or generally discontinuities. This implies that the Rankine-Hugoniot relation is coupled to the closure problem of turbulence [Biskamp, 2003]. When fluctuating fields are treated as a linear wave (small amplitude fluctuation), it is possible to describe the wave evolution across the shock by perturbing the Rankine-Hugoniot relation [McKenzie and Westphal, 1969, 1970; McKenzie, 1970; Westphal and McKenzie, 1969]. Turbulence, however, means large amplitude fluctuations and therefore one has to seek a non-perturbative method to solve the Rankine-Hugoniot relation in the presence of turbulent fields.

On the other hand, the Earth's bow shock, a standing shock wave located at about 20 Earth radii in front of the Earth, serves as an ideal, natural laboratory for studying the turbulence evolution across the shock. A number of spacecraft have visited the bow shock and its adjacent regions since 1960s and discovered various properties of the collisionless shock as well as turbulence in the solar wind.

The solar wind at 1 AU is believed to be in a fully developed turbulent state, as the frequency spectra of the magnetic field often exhibit a power law [Matthaeus and Goldstein, 1982; Matthaeus et al., 1982; Marsch and Tu, 1990]. The mean velocity of the solar wind is super-magnetosonic, typically about 400 km/s. The Earth's magnetosphere is a blunt obstacle to the solar wind and the bow shock is formed as the solar wind encounters this obstacle. Collisionless shocks at sufficiently high Mach number have a unique dissipation mechanism, in which a portion of the incoming particles are specularly reflected at the shock front. As a consequence the reflected particles stream backward (upstream against the incoming flow) along the magnetic field, forming an extended transition region in front of the shock [Paschmann et al., 1979, 1981]. This transition region is called the foreshock and it appears at shocks where the magnetic field is quasi-parallel to the shock normal direction. In contrast, when the magnetic field is quasi-perpendicular to the shock normal direction, the transition into the downstream region takes place only on a small scale, of the order of the ion gyro-radius. The solar wind is slowed and heated at the shock and enters the magnetosheath, where the flow is deflected to pass by the magnetosphere. A part of the magnetosheath flow reaches the cusp region behind the dayside magnetosphere.

Fluctuations in the foreshock and the magnetosheath are often interpreted within the framework of waves like normal modes in magnetohydrodynamics (MHD) or kinetic theory. There are a variety of studies based on this concept. Early spacecraft missions such as POLAR, Interball, AMPTE, ISEE and so on, have provided a lot of instructive observations regarding waves and instabilities, wave-particle interactions, properties of collisionless shocks (see reviews of Engebretson et al. [1994]; Paschmann et al. [2005] and reference therein). However, the definition of normal mode depends on the model of

plasma dynamics, e.g. MHD, two-fluid, cold plasma, or Vlasov model. And furthermore nonlinear effects are neglected when the modes are derived.

The Cluster mission [Escoubet et al., 2001], consisting of four spacecraft in polar orbit about the Earth, is ideal for studying waves and turbulence in the solar wind, the foreshock, and the magnetosheath, since measuring the particles and fields at four points in space enables one to distinguish between temporal and spatial variations and therefore to derive the spatial properties of various phenomena. One of its applications is to experimentally determine the dispersion relations [Narita et al., 2003; Narita and Glassmeier, 2005]. The energy spectra of the magnetic field fluctuations are directly determined in the wave number domain (hereafter the wave number spectra) in the regions from the solar wind to the foreshock, the magnetosheath, and the cusp. The interaction between solar wind turbulence and the bow shock is studied by tracing the evolution of the wave number spectra across the shock. For this purpose we introduce a decomposition method of magnetic field fluctuations into three distinct components: a two-dimensional component, an Alfvénic component, and a compressible component. The idea of the field decomposition is motivated by long-standing questions about the nature of the symmetries of solar wind turbulence, viz., whether or not turbulence is two-dimensional or Alfvénic [Matthaeus et al., 1990; Bieber et al., 1994, 1996]. This three-component model was originally introduced by Matthaeus and Ghosh [1999] and defined on the basis of the divergence-free nature of the magnetic field in spirit of turbulence. It is independent from the choice of dynamics models or normal modes. In our study the decomposition method is integrated with the estimator of the wave number spectra, providing the relative energy contributions of these components. Section 2 describes the estimators of the wave number spectra

The analysis method is then applied to the Cluster observations in section 3. The results are discussed in section 4. Section 5 concludes the text.

2. Spectral estimators

2.1. Decomposition of fluctuation

Magnetic field fluctuations under a background field can be in general decomposed into three components: a two-dimensional component, an Alfvénic component, and a compressible component. The two-dimensional component is an incompressible fluctuation associated with a wave vector perpendicular to the background magnetic field. This component is referred to as two-dimensional, since both the fluctuation and the wave vector are confined to the perpendicular plane to the background magnetic field. The Alfvénic component is also an incompressible fluctuation but is associated with a parallel (or anti-parallel) wave vector, representing an intuitive picture of an Alfvén wave propagating along the magnetic field. The compressible component represents a magnetic field fluctuation parallel to the background field and a perpendicular wave vector. Fig. 1 displays the fluctuations and the wave vectors of the three components. While the two-dimensional and the compressible component are linearly polarized, the (finite amplitude) Alfvénic component has two degrees of freedom in polarization. Therefore the Alfvénic component can be linearly, elliptically, or circularly polarized.

This representation with three components is convenient for studying turbulent fields for several reasons. One is the fact that the three components describe any magnetic field fluctuations uniquely and completely. The second reason is that this representation is based only on the divergence-free nature of the magnetic field and is free from the concept of wave modes. It is of course possible to decompose the fluctuations into the

normal mode of magnetohydrodynamics (MHD) [Glassmeier et al., 1995], but then one has to justify that the MHD picture is applicable to the fluctuation of interest. The third reason is that the fluctuation energy is given as a sum of the energy of the three components.

The three-component model can be understood as follows. First we separate the wave vector into two parts: parallel and perpendicular to the background magnetic field

$$\mathbf{k} = \begin{pmatrix} k_\perp \\ 0 \\ 0 \end{pmatrix} + \begin{pmatrix} 0 \\ 0 \\ k_\parallel \end{pmatrix}. \tag{1}$$

Here we choose the mean-field aligned (MFA) coordinate system in which the x and z axis are perpendicular and parallel to the background field $\mathbf{B}_0$ (assumed to be constant). The magnetic field fluctuation satisfies the divergence-free equation, yielding the condition $\mathbf{k} \cdot \delta\mathbf{B} = 0$ for the spatial periodic fluctuations. The fluctuation $\delta\mathbf{B}$ for the parallel and the perpendicular wave vectors are expressed as

$$\delta\mathbf{B}^{(k\perp)} = \begin{pmatrix} 0 \\ \delta B_t \\ \delta B_\parallel \end{pmatrix} \tag{2}$$

$$\delta\mathbf{B}^{(k\parallel)} = \begin{pmatrix} \delta B_{\perp 1} \\ \delta B_{\perp 2} \\ 0 \end{pmatrix}, \tag{3}$$

respectively. Here δB_t denotes the two-dimensional component. The subscript t stands for the transverse direction to the wave vector (and also perpendicular to the background field). $\delta B_\parallel$ denotes the compressible component, and $\delta B_{\perp 1}$ and $\delta B_{\perp 2}$ denote the two Alfvénic components. It is worthwhile to note that one does not need to assume an axisymmetry. The total fluctuation $\delta\mathbf{B}$ is hence obtained by adding Eq. (2) and (3),

$$\delta\mathbf{B} = \begin{pmatrix} \delta B_{\perp 1} \\ \delta B_{\perp 2} + \delta B_t \\ \delta B_\parallel \end{pmatrix}. \tag{4}$$

We define the total fluctuation energy by the trace of the matrix $\langle \delta\mathbf{B}\delta\mathbf{B}\rangle$, where the angular bracket denotes the averaging. In this paper, the averaging is made in the time domain. On the assumption that the three fluctuation components are mutually incoherent, the total fluctuation energy is given as a superposition of the energy of the three components,

$$E = \mathrm{tr}\langle \delta\mathbf{B}\delta\mathbf{B}^T\rangle \tag{5}$$

$$= \Big(\langle|\delta B_{\perp 1}|^2\rangle + \langle|\delta B_{\perp 2}|^2\rangle\Big) + \langle|\delta B_t|^2\rangle + \langle|\delta B_{\parallel}|^2\rangle. \tag{6}$$

The first two terms in the round bracket represent the energy of the Alfvénic component, while the third and the last term represent that of the two-dimensional and the compressible components, respectively.

2.2. Projection into wave vector space

The second pillar of the analysis is to estimate the energy spectra directly in the wave number domain. It is of course ideal to have as many spacecraft available as possible to Fourier transform the fluctuations from the spatial coordinates into wave numbers. It is true that the four measurement points provided by Cluster, from this point of view, are too few for performing the Fourier transform into the wave number domain, but it is still possible to use an alternative method that substitutes for the role of the Fourier transform by estimating the fluctuation amplitude as a function of frequency and wave vector. Several attempts have already been made to determine the wave number spectra from Cluster observations [Narita et al., 2006, 2008; Sahraoui et al., 2006].

The determination of the wave number spectrum makes use of a projection of the cross spectral density (CSD) matrix into the wave vector space. The CSD matrix is obtained

from the measurements as

$$\mathsf{M}(\omega) = \frac{1}{T}\langle \mathbf{S}(\omega)\mathbf{S}^{\dagger}(\omega)\rangle, \tag{7}$$

where ω denotes the (angular) frequency, T the length of the measurement time, and the dagger † the Hermitian conjugate. $\mathbf{S}(\omega)$ is the state vector of the measured magnetic field fluctuations that are Fourier transformed from the time domain to the frequency domain. Here the background field is assumed to be constant. In the case of the Cluster magnetic field measurement, the state vector consists of 12 elements (3 magnetic field components times 4 measurement points):

$$\mathbf{S}(\omega) = \begin{pmatrix} \mathbf{B}_1(\omega) \\ \mathbf{B}_2(\omega) \\ \mathbf{B}_3(\omega) \\ \mathbf{B}_4(\omega) \end{pmatrix}, \tag{8}$$

where the subscript refers to the measurement point (i.e., spacecraft). The CSD matrix (Eq. 7) is projected into a 3×3 matrix using a weight matrix $\mathsf{W}(\omega, \mathbf{k})$:

$$\mathsf{E}(\omega, \mathbf{k}) = \mathsf{W}^{\dagger}(\omega, \mathbf{k})\mathsf{M}(\omega)\mathsf{W}(\omega, \mathbf{k}). \tag{9}$$

Here we choose the minimum variance weight, which has the form

$$\mathsf{W}(\omega, \mathbf{k}) = \mathsf{M}^{-1}(\omega)\mathsf{H}(\mathbf{k})\mathsf{V}(\mathbf{k}) \left[\mathsf{V}^{\dagger}(\mathbf{k})\mathsf{H}^{\dagger}(\mathbf{k})\mathsf{M}^{-1}(\omega)\mathsf{H}(\mathbf{k})\mathsf{V}(\mathbf{k})\right]^{-1}, \tag{10}$$

where $\mathsf{H}(\mathbf{k})$ is a 12×3 matrix and called the steering matrix:

$$\mathsf{H}(\mathbf{k}) = \begin{pmatrix} \mathsf{I}\exp(i\mathbf{k}\cdot\mathbf{r}_1) \\ \mathsf{I}\exp(i\mathbf{k}\cdot\mathbf{r}_2) \\ \mathsf{I}\exp(i\mathbf{k}\cdot\mathbf{r}_3) \\ \mathsf{I}\exp(i\mathbf{k}\cdot\mathbf{r}_4) \end{pmatrix} \tag{11}$$

with I the 3×3 unit matrix. The steering matrix reflects the periodic spatial pattern characterized by the wave vector $\mathbf{k}$ with amplitude unity. The matrix $\mathsf{V}(\mathbf{k})$ in Eq. (10) is given as

$$\mathsf{V}(\mathbf{k}) = \mathsf{I} + \frac{\mathbf{kk}}{k^2}, \tag{12}$$

where $k = |\mathbf{k}|$. The weight matrix (Eq. 10) is optimized to minimize the projected matrix (Eq. 9) under two constraints, the weight matrix satisfying the unit gain condition:

$$\mathsf{W}^{\dagger}(\omega, \mathbf{k})\mathsf{H}(\mathbf{k}) = \mathsf{I}, \tag{13}$$

and, second, the divergence-free nature of the magnetic field, which results in the matrix $\mathsf{V}(\mathbf{k})$. It is worthwhile to note that the weight matrix is determined by the measurement itself (the CSD matrix in Eq. 7). The matrix projected into the wave vector space is therefore given analytically from Eq. (9) and (10) as

$$\mathsf{E}(\omega, \mathbf{k}) = \left[\mathsf{V}^{\dagger}(\mathbf{k})\mathsf{H}^{\dagger}(\mathbf{k})\mathsf{M}(\omega)\mathsf{H}(\mathbf{k})\mathsf{V}(\mathbf{k})\right]^{-1}. \tag{14}$$

This estimator of $\mathsf{E}(\omega, \mathbf{k})$ is referred to as the wave telescope (or k-filtering) [Pinçon and Lefeuvre, 1991; Motschmann et al., 1996; Glassmeier et al., 2001] and is applied to determine the wave number spectra. The projection in Eq. (9) does not change the units of the matrix elements, and therefore the projected matrix $\mathsf{E}(\omega, \mathbf{k})$ has the same unit as that of the CSD matrix (Eq. 7), namely $\mathrm{nT}^2/\mathrm{Hz}$ in the case of the magnetic field. To obtain the wave number spectra, the unit of the projected matrix is adapted by integration over frequency and then division by the grid size of the wave vector space Δk such that the unit of the spectrum is given as squared amplitude per wave number, $\mathrm{nT}^2\,\mathrm{km}$.

2.3. Spectrum of two-dimensional component

The wave number spectrum for the two-dimensional component is obtained in several steps. (1) The matrix E is determined in the mean-field coordinate system at various perpendicular wave vectors $\mathbf{k} = (k_\perp \cos\phi, k_\perp \sin\phi, 0)$ and frequencies, where ϕ denotes the azimuthal angle about the background field direction (z axis). (2) The xy plane is rotated about the z axis to orient the x axis in the wave vector direction, such that the

y axis is perpendicular to the background field and tranverse to the wave vector. (3) The spectral energy in the y direction is obtained from the rotated matrix as a function of frequency, perpendicular wave number, and azimuthal angle, $E_{yy}(\omega, k_\perp, \phi)$. (4) The spectrum E_{yy} is integrated over frequency in the flow rest frame $\omega_{re} = \omega_{sc} - \mathbf{k}\cdot\mathbf{V}$ and the azimuthal angles, which gives the spectrum in units of squared amplitude (nT^2). (5) The spectrum is transformed into the spectral density in the wave number domain ($\mathrm{nT}^2\,\mathrm{km}$). The transformation is made by dividing the spectrum by the grid size of the wave number. We use in the present study a logarithmically equidistant grid such that the grid size is proportional to the wave number itself, $\Delta k_\perp \propto k_\perp$. In short, the spectral estimator for the two-dimensional component is given as

$$E_{2d}(k_\perp) = \frac{1}{\Delta k_\perp}\int_0^{2\pi} d\phi \int d\omega E_{yy}(\omega, k_\perp, \phi). \tag{15}$$

2.4. Spectrum of Alfvénic component

The wave number spectrum for the Alfvénic component is determined in the following steps. (1) The matrix E is determined in the mean-field coordinate system at various parallel and anti-parallel wave vectors $\mathbf{k} = (0, 0, \pm k_\parallel)$ and frequencies. (2) The energy of the perpendicular fluctuation is obtained by summing the x and y diagonal components of the matrix, $E_\perp(\omega, \pm k_\parallel) = E_{xx}(\omega, \pm k_\parallel) + E_{yy}(\omega, \pm k_\parallel)$. (3) The energies for the parallel and the anti-parallel wave vectors obtained in the step 2 are summed and integrated over the rest frame frequency. (4) The spectrum is divided by the grid size of the parallel wave number. The spectral estimator is thus given as

$$E_{alf}(k_\parallel) = \frac{1}{\Delta k_\parallel}\int d\omega \left[E_\perp(\omega, k_\parallel) + E_\perp(\omega, -k_\parallel)\right]. \tag{16}$$

2.5. Spectrum of compressible component

The wave number spectrum for the compressible component is obtained by replacing E_{yy} (perpendicular fluctuation energy) by E_{zz} (parallel fluctuation energy) in the estimator of the spectrum of the two-dimensional component (Eq. 15). The estimator is given as

$$E_{cmp}(k) = \frac{1}{\Delta k_\perp} \int_0^{2\pi} d\phi \int d\omega E_{zz}(\omega, k_\perp, \phi). \tag{17}$$

3. Measurement of wave number spectra

3.1. Cluster observations

We apply the spectral decomposition method to the Cluster observations and obtain the wave number spectra as well as the relative energy contributions of the three components. We use the magnetic field data from the Cluster fluxgate magnetometer (FGM) [Balogh et al., 2001] (time resolution 22 vec/s) and determine the wave number spectra in various regions from two bow shock crossings for the mission phase with 100 km spacecraft separation. The orbit of the first crossing (orbit A) encountered (1) the solar wind, (2) the foreshock, and (3) the magnetosheath. The orbit for the second crossing (orbit B) encountered (4) the solar wind, (5) the magnetosheath, and (6) the magnetospheric cusp region. While the first orbit represents a crossing of the quasi-parallel shock (Alfvén Mach number 7.6, angle between the shock normal and the upstream magnetic field 30.5 deg), the second one represents a crossing of the quasi-perpendicular shock (Alfvén Mach number 4.0, angle 75.7 deg). Fig. 2 and 3 display the schematic and the actual orbits of Cluster. Fig. 4 displays the observed magnetic field magnitude for the two shock crossings. The orbit A is inbound (from the solar wind to the magnetosphere) and encountered the shock crossing at about 1600 UT and the magnetopause crossing at about 2130 UT. We use the

interval (1) Feb. 11, 2002, 1730–2030 UT for the solar wind, (2) Feb. 12, 2002, 0630–1230 UT for the foreshock, and (3) 1615–2100 UT for the magnetosheath. The orbit B is outbound. After exiting the nightside magnetosphere just before 0900 UT, the spacecraft re-entered the magnetosphere on the dayside at about 1000 UT and encountered the dayside magnetopause and the shock at about 1015 UT and 1350 UT, respectively. We use the intervals (4) Mar. 4, 2002, 1415–1615 UT for the solar wind, (5) 1015–1330 UT for the magnetosheath, and (6) 0900–0945 UT for the cusp. It is of course possible to split the time interval of analysis into more sub-intervals, but we aim to determine average properties of fluctuations from each region and for this purpose we use the whole intervals.

We determine the wave number spectra and the energy contributions of the three components (two-dimensional, Alfvénic, and compressible components) for the six regions from the solar wind to the cusp. The spectra are determined at various wave numbers in the parallel and the perpendicular direction to the background magnetic field using the logarithmically equidistant grid (30 grid points within one order of magnitude of the wave number, which are chosen to be close enough such that the spectral curves are identified in the analysis), and then averaged over ensembles with 32 time sub-intervals. The discrete grid and the projection of the ensemble averaged CSD matrix result in smoothed spectral curves. The energy contributions are derived from the wave number spectra using Eq. 6. In the following subsections we present the wave number spectra, the frequency spectra, and the energy contributions in the solar wind, the foreshock, the magnetosheath, and the cusp.

3.2. Solar wind (orbits A and B)

The wave number spectrum in the solar wind for the orbit A is displayed in Fig. 5-(1). Most of the fluctuation energy is contributed by the two-dimensional component at various wave numbers. The compressible component has the second largest contribution, and the Alfvénic makes the weakest contribution. The two-dimensional component exhibits a power law spectrum with the index close to -5/3 up to the spectral break at the wave numbers about $k = 5 \times 10^{-3}\,\mathrm{km}^{-1}$ (marked with an arrow). The compressible and the Alfvénic component have also similar spectral curves, but the spectrum of the Alfvénic component is slightly steeper. The frequency spectrum displayed in Fig. 6-(1) exhibits the dominance of the perpendicular fluctuation to the background magnetic field, which agrees with the dominance of the two-dimensional component in the wave number spectrum. The spectral curve in the frequency domain is also a power law with the index close to -5/3, and the scale of the spectral break almost agrees with that in the wave number domain. In the frequency domain the break is identified at $f = 4 \times 10^{-1}\,\mathrm{s}^{-1}$, which corresponds to the wave numbers derived from Taylor's hypothesis at about $k = 5 \times 10^{-3}\,\mathrm{km}^{-1}$. Fig. 7-(1) displays the energy contribution of the three components in units of percentage. Up to the spectral break scale ($k \leq 5 \times 10^{-3}\,\mathrm{km}^{-1}$) the two-dimensional component occupies about 60% of the fluctuation energy, the Alfvénic component about 15-20%, and the compressible component about 20-25%. Beyond the spectral break scale the contribution of the compressible component increases rather suddenly toward higher wave numbers, whereas that of the two-dimensional component becomes smaller.

The wave number spectrum for the orbit B is displayed in Fig. 5-(4). The spectrum exhibits some similarities and on the other hand some differences from the spectrum of the

orbit A. The two-dimensional component dominates again in the spectrum and exhibits the power law with the index close to -5/3, but the spectrum of the Alfvénic and the compressible component almost degenerate, overlapping with each other. The frequency spectrum (Fig. 5-(4)) exhibits the -5/3 spectrum and the spectral break at the frequencies about $f = 2 \times 10^0\,\mathrm{s}^{-1}$, or at the wave numbers (derived from Taylor's hypothesis) about $k = 2 \times 10^{-1}\,\mathrm{km}^{-1}$. The break is not seen in the wave number spectrum, as the wave number of the spectral break scale is higher than the Nyquist wave number limit due to the spacecraft separation (100 km). The energy contribution is displayed in Fig. 7-(4), exhibiting 50-60% by the two-dimensional component, 20% by the Alfvénic component, and 20-30% by the compressible component.

3.3. Foreshock (orbit A)

The wave number spectrum in the foreshock is displayed in Fig. 5-(2). The spectrum is characterized by enhancement (or amplification) of the spectral power at various wave numbers. The spectra also exhibit a hump on an intermediate scale. The enhancement of the spectra is primarily seen in the Alfvénic and the compressible component, while the spectral power of the two-dimensional component does not change much. The enhancement of the Alfvénic component is so large that it almost reaches the spectrum of the two-dimensional component, especially in the range $10^{-3}\,\mathrm{km}^{-1} < k < 10^{-2}\,\mathrm{km}^{-1}$. The enhancement of the compressible component is also prominent. All the three components exhibit a moderate hump at the wave numbers about $k = 1 \times 10^{-3}\,\mathrm{km}^{-1}$. The hump may be interpreted as the so-called "30 second waves" often observed in the foreshock (e.g. Greenstadt et al. [1995]), as the frequency spectrum exhibits a peak at about $f = 5 \times 10^{-2}\,\mathrm{s}^{-1}$ in Fig. 6-(2). (In the present case the peak is at 20 seconds.) The

frequency spectrum also exhibit a spectral break at higher frequencies ($f \simeq 1 \times 10^0\,\mathrm{s}^{-1}$), but this break is not seen in the wave number spectra, again because its spatial scale is smaller than the spacecraft separation. The energy contribution is displayed in Fig. 7-(2). The two-dimensional component contributes about 40-45%, the Alfvénic component about 35-40%, and the compressible component about 20%.

3.4. Magnetosheath (orbits A and B)

The wave number spectrum in the magnetosheath for the orbit A is displayed in Fig. 5-(3). All three components are enhanced by one to two orders of magnitude by comparison with the foreshock spectrum. The spectral lines are gently curved such that the energy decays more rapidly toward larger wave numbers. The curved spectra are also identified in the frequency spectra in Fig 6-(3). The energy contribution is displayed in Fig. 7-(3). The compressible component has the dominant contribution, about 45%, while the two-dimensional and the Alfvénic component contribute about 35% and 20%, respectively.

The spectrum for the orbit B is displayed in Fig. 5-(5) and is similar to that from the orbit A. The spectral lines are again slightly curved and the three components are enhanced from the solar wind spectrum (Fig. 5-(4)) by one to two orders of magnitude. The two-dimensional component dominates the spectrum, but the difference from the compressible component (the second dominant component) is not much. The frequency spectrum displayed in Fig. 6-(5) exhibits a hump at the Taylor scale wave number about $k = 5 \times 10^{-3}\,\mathrm{km}^{-1}$, but the hump is not clearly seen in the wave number spectrum. However, it should be noted that Taylor's hypothesis fails in the magnetosheath, since the wave propagation speed is larger than the flow speed in the post-shock region and therefore the frequency spectrum does not immediately reflect the form of the wave number

spectrum. The energy contribution is displayed in Fig. 7-(5). The two-dimensional component contributes about 45%, the Alfvénic component about 20%, and the compressible component about 35%.

3.5. Cusp (orbit B)

The wave number spectrum in the cusp is displayed in Fig. 5-(6). At smaller to intermediate wave numbers the spectrum is dominated by the compressible component, while at higher wave numbers it is dominated by the two-dimensional component. The turnover scale is about $10^{-2}\,\mathrm{km}^{-1}$. The Alfvénic component is much diminished by one to two orders of magnitude from the magnetosheath spectrum. The frequency spectrum in Fig. 6-(6) exhibits curved lines with the perpendicular fluctuation dominant, but these curves do not reflect the wave number spectra any more, since Taylor's hypothesis fails again in the cusp region. The energy contribution in Fig. 7-(6) shows that the Alfvénic component contributes only about 5-10%. The compressible component dominates at smaller and intermediate wave numbers by about 60% and becomes diminished to about 35%. The two-dimensional is enhanced from 25 to 55% toward higher wave numbers in return.

3.6. Coherence

The assumption of incoherent fluctuations used in the analysis is examined, too. The existence of coherence brings an additional term in the expression of the energy decomposition (Eq. 6), that is the coupling of the two-dimensional and the Alfvénic component, $\langle \delta B_{\perp 2} \delta B_t \rangle$ Fig. 8 displays the histogram of coherence

$$\gamma(k_\parallel, k_\perp) = \frac{|\langle \delta B_{\perp 2}(k_\parallel) \delta B_t^*(k_\perp) \rangle|}{\sqrt{\langle |\delta B_{\perp 2}(k_\parallel)|^2 \rangle} \sqrt{\langle |\delta B_t(k_\perp)|^2 \rangle}}$$

between these two components at various wave numbers for the six regions. The result is that the coherence is small enough in all the regions. The coherence varies at most up to 0.05 but mostly smaller than 0.01.

3.7. Summary of the results

To summarize, first of all, the two-dimensional component is a major contributor in the fluctuation energy from the solar wind to the cusp. In the smallest case its contribution is about 35% in the magnetosheath behind the quasi-parallel shock and in the largest case it is about 60% in the solar wind. The two-dimensional component dominates in the solar wind and exhibits a power law spectrum with the index close to -5/3, which justifies the arguments of Matthaeus et al. [1990] and Bieber et al. [1994, 1996]. There are transitions both in the spectral power (that is proportional to the squared amplitude) and in the relative energy contributions as the solar wind enters the magnetosheath. For the quasi-parallel shock crossing the three components are amplified first in the foreshock and then further amplified in the magnetosheath. The Alfvénic component is prominently enhanced in the foreshock and the compressible component is most enhanced in the magnetosheath. For the quasi-perpendicular shock crossing the compressible component is also most enhanced in the magnetosheath, while in the cusp region the Alfvénic component is suppressed.

4. Discussion

As demonstrated in section 3, the magnetic fluctuation spectra observed in the foreshock, the magnetosheath, and the cusp are all enhanced by comparison with spectra observed in the upstream solar wind. Two likely sources for these enhancements are plasma

instabilities and amplification of fluctuations at the bow shock (See discussion below). In the foreshock, electron-beam and ion-beam modes are the most likely instabilities, because the bow shock is a source of heated electrons and reflected ions. In the frequency range of concern to us, the most likely mode to grow is the electromagnetic ion/ion right-hand resonant instability. This has been confirmed observationally by Watanabe and Terasawa [1984]; Fuselier et al. [1986a, b] using single spacecraft methods and recently by Narita et al. [2003]; Narita and Glassmeier [2005]; Narita et al. [2007] using multi-spacecraft methods of Cluster. Winske and Leroy [1984] use numerical simulations and show the relation between the diffuse ion component and this instability. Linear theory [Gary, 1993] shows that the instability has maximum growth at $kc/\omega_{pp} < 1$ and at $\mathbf{k} \times \mathbf{B}_0 = 0$ ($k = |\mathbf{k}|$, c the light speed, ω_{pp} the proton plasma frequency), so that enhanced fluctuations from this instability should have properties of the Alfvénic component defined in section 2. Magnetosheath plasma shows the consequences of magnetic compression and heating at the shock, so that the primary characteristic of proton distributions in this regime is a strong $T_\perp/T_\parallel > 1$ anisotropy. This anisotropy leads to the growth of both electromagnetic ion cyclotron and mirror-mode fluctuations, e.g. Anderson and Fuselier [1993], with the mirror instability often dominating the high-β plasmas near and downstream of the shock. The mirror instability has maximum growth at directions strongly oblique to $\mathbf{B}_0$ and has a strong $\delta B_\parallel$ component [Gary, 1993], so that enhanced fluctuations from this growing mode should have properties of the compressible component defined in section 2. In our case the plasma parameter β is 4.13 and 1.48 in the magnetosheath for the orbit A and B, respectively. Though β for the orbit B is only moderately high, the relationship between β and the mirror mode interpretation is in accord with Anderson and Fuselier [1993].

There are two possible major explanations why the fluctuations are amplified as the solar wind undergoes the shock transition. One possibility is that waves are excited by instabilities in the foreshock and the magnetosheath. This interpretation accounts for the enhancement of the Alfvénic component in the foreshock and the compressible component in the magnetosheath. Indeed, the dispersion analysis of Cluster shows the existence of the magnetosonic/whistler mode in the foreshock and the mirror mode in the magnetosheath [Narita et al., 2003; Narita and Glassmeier, 2005]. The magnetosonic/whistler mode has the wave field that is propagating along the magnetic field at the Alfvén speed at lower frequencies, so that this wave field probably contributes to the Alfvénic component in our analysis. This accounts for the enhancement of the Alfvénic component in the foreshock. Also, the mirror mode is a non-propagating, compressible fluctuation associated with the wave vector nearly perpendicular to the magnetic field, therefore the enhancement of the compressible component in the magnetosheath can be explained by the excitation of the mirror mode.

The second possible explanation is that the fluctuations in the solar wind are amplified at the shock independent of any instabilities. The interaction of the MHD waves with the shock wave can be analytically modeled and solved by perturbing the Rankine-Hugoniot relations to the first order. In general, the interaction results in reflection and transmission of the incident wave across the shock. The analysis suggests that the magnetic field amplitude of an Alfvén wave incident in the shock-upstream region is enhanced by a factor of unity or three, depending on the sense of wave propagation in the upstream and downstream region with respect to the shock normal direction [McKenzie and Westphal, 1969, 1970; McKenzie, 1970; Hassam, 1978]. The analysis also predicts that the ampli-

fication of a fast magnetosonic wave is about a factor of four [Westphal and McKenzie, 1969]. Therefore we estimate naively the jump of the spectral power by factors $10 - 20$ across the shock, which is, interestingly, close to our measurement. (Note that energy is proportional to squared amplitude of the field.) It is also worthwhile to mention that there are a variety of possible scenarios within the framework of the wave picture: amplification or mode conversion of waves at the bow shock and the magnetopause; generation of waves due to local instabilities associated with these discontinuities; reflected waves; standing waves in front of the magnetopause.

5. Conclusions

We summarize our principal results as follows.

(1) The two-dimensional component is a major contributor to the fluctuation energy not only in the solar wind but also in the foreshock, the magnetosheath, and the cusp region. (2) The two-dimensional component dominates in the solar wind, and its wave number spectrum is close to the -5/3 spectrum. (3) The transition from the solar wind to the magnetosheath is accompanied by two effects. One is the amplification of the fluctuations in all the three components. The spectral amplification across the shock is by one to two orders of magnitude, which is close to the estimate based on the perturbed Rankine-Hugoniot relation. Another effect is that energy contribution of the three components is reconfigured in the foreshock, the magnetosheath, and the cusp. The foreshock and the magnetosheath exhibit more enhancement in the Alfvénic and the compressible component, respectively. This suggests that waves are excited in situ by instabilities. The enhanced compressible component in the magnetosheath is seen for both the quasi-parallel

and the quasi-perpendicular shock crossing. In the cusp region, the Alfvénic component is suppressed.

Acknowledgments. The work of YN and KHG was financially supported by Bundesministerium für Wirtschaft und Technologie and Deutsches Zentrum für Luft- und Raumfahrt, Germany, under contract 50OC0103. We thank H. Rème and I. Dandouras for providing the ion data of Cluster. The work of SPG was supported by the Los Alamos National Laboratory LDRD Program and by the NASA Solar and Heliospheric SR&T Program.

References

Anderson, B. J., and S. A. Fuselier, Magnetic pulsations from 0.1 to 4.0 Hz and associated plasma properties in the earth's subsolar magnetosheath and plasma depletion layer, *J. Geophys. Res., 98* , 1461–1479 ,1993.

Balogh, A., C. M. Carr, M. H. Acuña, M. W. Dunlop, T. J. Beek, P. Brown, K.-H. Fornaçon, E. Georgescu, K.-H. Glassmeier, J. Harris, G. Musmann, T. Oddy, and K. Schwingenschuh, The Cluster magnetic field investigation: overview of in-flight performance and initial results *Ann. Geophys., 19* , 1207–1217 ,2001.

Bieber, J. W., W. H. Matthaeus, C. W. Smith, W. Wanner, M.-B. Kallenrode, and G. Wibberenz, Proton and electron mean free paths: The Palmer consensus revisited, *Astrophys. J., 420*, 294–306, 1994.

Bieber, J. W., W. Wannger, and W. H. Matthaeus, Dominant two-dimensional solar wind turbulence with implications for cosmic ray transport, *J. Geophys. Res., 101*, 2511–2522, 1996.

Biskamp, D., *Magnetohydrodynamic turbulence*, pp. 100–102, Cambridge Univ. Press, Cambridge, 2003.

Engebretson, M. J., K. Takahashi, and M. Scholer (eds.), *Solar wind sources of magnetospheric ultra-low-frequency waves*, Geophys. Monograph 81, American Geophysical Union, Washington, DC, 1994.

Escoubet, C. P., M. Fehringer, and M. Goldstein, The Cluster mission, *Ann. Geophys., 19*, 1197–1200, 2001.

Fermi, E., On the origin of the cosmic radiation *Phys. Rev., 75*, 1169–1174, 1949.

Fuselier, S. A., M. F. Thomsen, J. T. Gosling, S. J. Bame, and C. T. Russell, Gyrating and intermediate ion distributions upstream from the earth's bow shock, *J. Geophys. Res., 91*, 91–99, 1986a.

Fuselier, S. A., M. F.Thomsen, S. P. Gary, S. J. Bame, and C. T. Russell, The phase relationship between gyrophase-bunched ions and MHD-like waves, *Geophys. Res. Lett., 13*, 60–63, 1986b.

Gary, S. P., *Theory of Space Plasma Microinstabilities*, Cambridge, 1993.

Glassmeier, K.-H., U. Motschmann, and R. von Stein, Mode recognition of MHD wave fields at incomplete dispersion measurements, *Ann. Geophys., 13*, 76–83, 1995.

Glassmeier, K.-H., U. Motschmann, M. Dunlop, A. Balogh, M. H. Acuña, C. Carr, G. Musmann, K.-H. Fornaçon, K. Schweda, J. Vogt, E. Georgescu, and S. Buchert, Cluster as a wave telescope - first results from the fluxgate magnetometer, *Ann. Geophys., 19*, 1439–1447, 2001.

Greenstadt, E. W., G. Le, R. J. Strangeway, ULF waves in the foreshock, *Adv. Space Res., 15*, 71–84, 1995.

Hassam, A. B., Transmission of Alfvén waves through the Earth's bow shock: theory and observation, *J. Geophys. Res., 83*, 643–653, 1978.

Marsch, E., and C.-Y. Tu, On the radial evolution of MHD turbulence in the inner heliosphere, *J. Geophys. Res., 95*, 8211–8229, 1990.

Matthaeus, W. H., and M. L. Goldstein, Measurement of the rugged invariants of magnetohydrodynamic turbulence in the solar wind *J. Geophys. Res., 87*, 6011–6028, 1982.

Matthaeus, W. H., M. L. Goldstein, and C. Smith, Evaluation of magnetic helicity in homogeneous turbulence, *Phys. Rev. Lett., 48*, 1256–1259, 1982.

Matthaeus, W. H., M. L. Goldstein, and D. A. Roberts, Evidence for the presence of quasi-two-dimensional nearly incompressible fluctuations in the solar wind *J. Geophys. Res., 95*, 20,673–683, 1990.

Matthaeus, W. H., and S. Ghosh, Spectral Decomposition of Solar Wind Turbulence: Three-Component Model, in *Solar Wind Nine, Proceedings of the Ninth International Solar Wind Conference, Nantucket, MA, October 1998*, pp. 519, S. R. Habbal, R. Esser, J. V. Hollweg, and P. A. Isenberg (eds.), AIP Conference Proceedings, 471, 1999.

McKenzie, J. F., and K. O. Westphal, Transmission of Alfvén waves through the Earth's bow shock, *Planet. Space Sci., 17*, 1029–1037, 1969.

McKenzie, J. F., Hydromagnetic wave interaction with the magnetopause and the bow shock, *Planet. Space Sci., 18*, 1–23, 1970.

McKenzie, J. F., and K. O. Westphal, Interaction of hydromagnetic waves with hydromagnetic shocks, *Phys. Fluids., 13*, 630–640, 1970.

Motschmann, U. T. I. Woodward, K. H. Glassmeier, D. J. Southwood, and J. L. Pinçon, Wavelength and direction filtering by magnetic measurements at satellite arrays: Gen-

eralized minimum variance analysis, *J. Geophys. Res., 101*, 4961–4966, 1996.

Narita, Y., K.-H. Glassmeier, S. Schäfer, U. Motschmann, K. Sauer, I. Dandouras, K.-H. Fornaçon, E. Georgescu, and H. Rème, Dispersion analysis of ULF waves in the foreshock using cluster data and the wave telescope technique, *Geophys. Res. Lett., 30*, SSC 43–1, doi:10.1029/2003GL017432, 2003.

Narita, Y. and K.-H. Glassmeier, Dispersion analysis of low-frequency waves through the terrestrial bow shock, *J. Geophys. Res., 110*, A12215, doi:10.1029/2005JA011256, 2005.

Narita, Y., K.-H. Glassmeier, and R. A. Treumann, Wave-number spectra and intermittency in the terrestrial foreshock region, *Phys. Rev. Lett.*, **97**, 191101, doi:10.1103/PhysRevLett.97.191101, 2006a.

Narita, Y., K.-H. Glassmeier, M. Fränz, Y. Nariyuki, and T. Hada, Observations of linear and nonlinear processes in the foreshock wave evolution, *Nonlin. Processes Geophys., 14*, 361–371, 2007.

Narita, Y., K.-H. Glassmeier, S. P. Gary, M. L. Goldstein, and R. A. Treumann, Wave-vector dependence of magnetic turbulence spectrain the solar wind, *Phys. Rev. Lett.*, submitted, 2008.

Paschmann, G., N. Sckopke, S. J. Bame, J. R. Asbridge, J. T. Gosling, C. T. Russell, and E. W. Greenstadt, Association of low-frequency waves with suprethermal ions in the upstream solar wind, *Geophys. Res. Lett., 6*, 209–212, 1979.

Paschmann, G., N. Sckopke, I. Papamastorakis, J. R. Asbridge, S. J. Bame, and J. T. Gosling, Characteristics of reflected and diffuse ions upstream of from the Earth's bow shock, . *J. Geophys. Res., 86*, 4355–4364, 1981.

Paschmann, G., S. J. Schwartz, C. P. Escoubet, and S. Haaland, *Outer magnetospheric boundaries: Cluster results*, Space Sciences Series of ISSI, 20, Springer, the Netherlands, 2005.

Pinçon, J. L. and F. Lefeuvre, Local characterization of homogeneous turbulence in a space plasma from simultaneous measurements of field components at several points in space, *J. Geophys. Res., 96*, 1789–1802, 1991.

Sahraoui, F., G. Belmont, L. Rezeau, N. Cornilleau-Wehrlin, J. L. Pinçn, and A. Balogh, Anisotropic turbulent spectra in the terrestrial magnetosheath as seen by the Cluster spacecraft, *Phys. Rev. Lett., 96*, 075002, doi:10.1103/PhysRevLett.96.075002, 2006.

Watanabe, Y., and T. Terasawa, *J. Geophys. Res., 89*, 6623–6630, 1984.

Westphal, K. O., and J. F. McKenzie, Interaction of magnetoacoustic and entropy waves with normal magnetohydrodynamic shock waves, *Phys. Fluids, 12*, 1228–1236, 1969.

Winske, D., and M. M. Leroy, Diffuse ions produced by electromagnetic ion beam instabilities, *J. Geophys. Res., 89*, 2673–2688, 1984.

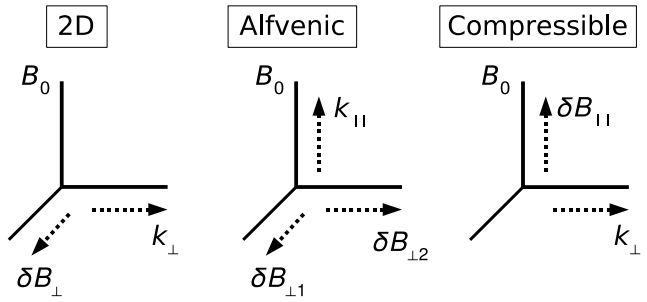

Figure 1. Three magnetic field components under the mean magnetic field.

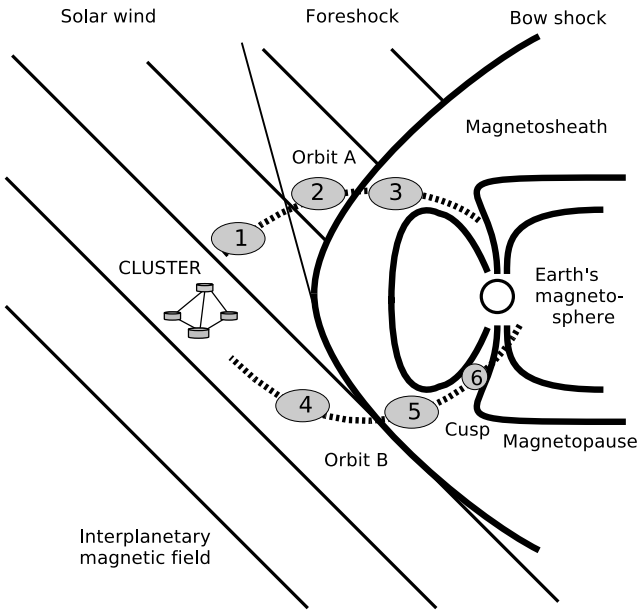

Figure 2. Illustration of of Cluster orbits through the Earth's bow shock. Orbit A and B stand for the crossing of the quasi-parallel and the quasi-perpendicular shock, respectively. The numbered areas denote the locations used for the investigation of the wave number spectra.

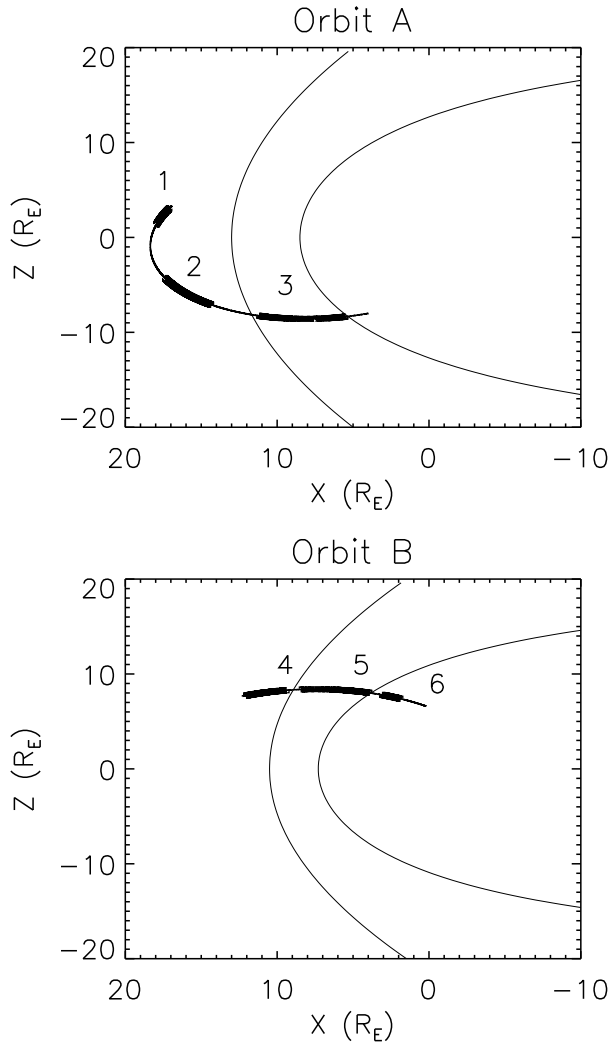

Figure 3. Actual orbit of Cluster in the XZ plane of GSE coordinate system. The outer and inner curves represent the bow shock and the magnetopause.

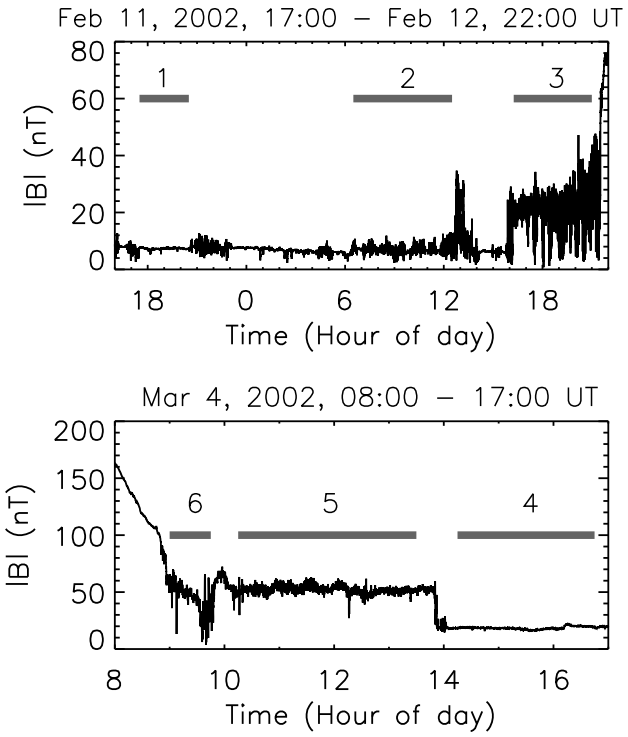

Figure 4. Time series plots of the magnetic field magnitude for orbit A (top) and B (bottom). The numbered intervals correspond to the numbered areas in Fig. 2 and 3.

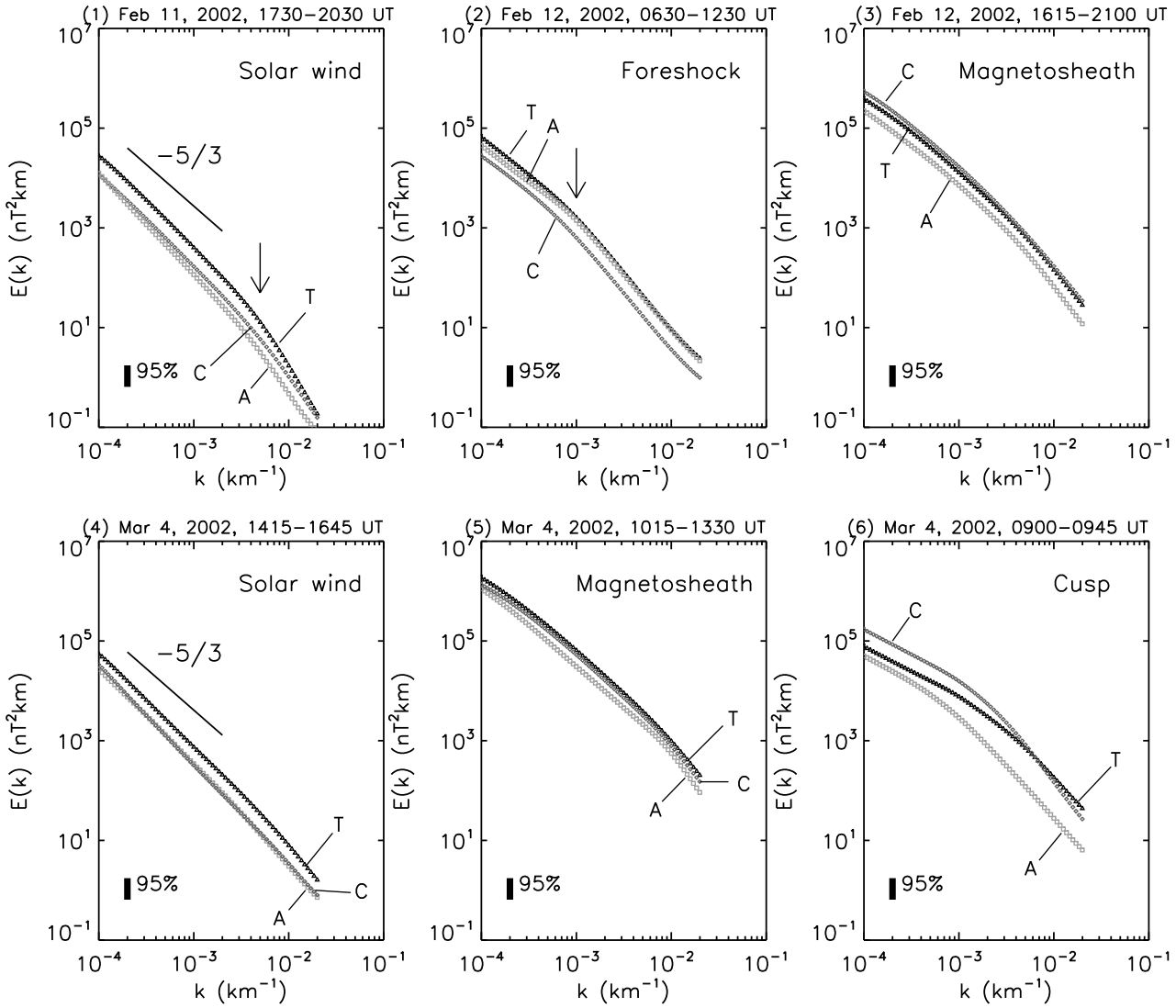

Figure 5. Wave number spectra of magnetic field fluctuations for the two-dimensional component (T), the Alfvénic component (A), and the compressible component (C). Vertical bars stand for the interval of 95% confidence of the spectra. Arrows point a hump or a spectral break.

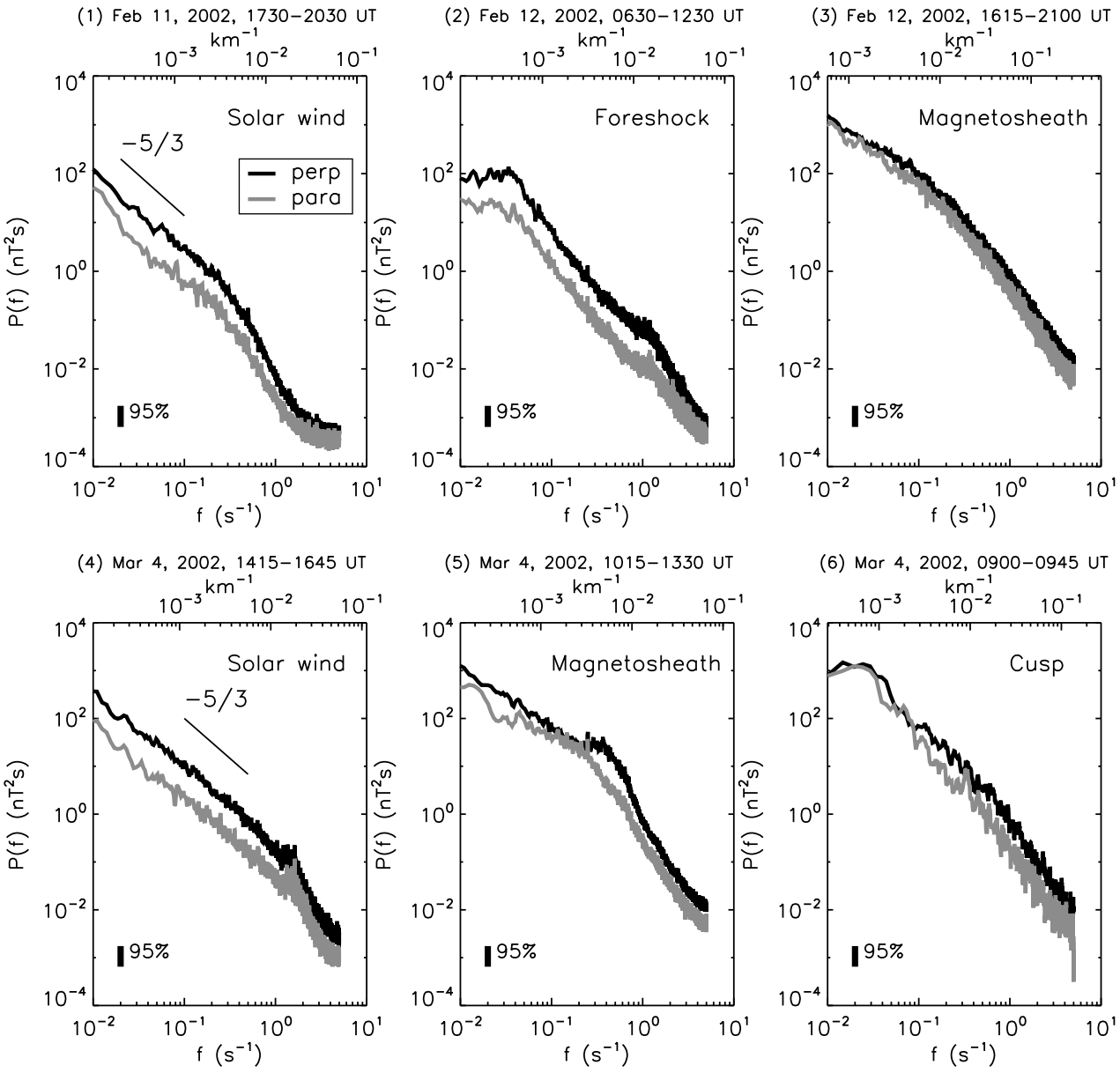

Figure 6. Frequency spectra of perpendicular (in black) and compressible magnetic field fluctuations (gray) determined from the measurements of the Cluster-1 spacecraft. The corresponding wave numbers derived from Taylor's hypothesis are attached on the top of each panel. The solid vertical bars stand for the confidence interval.

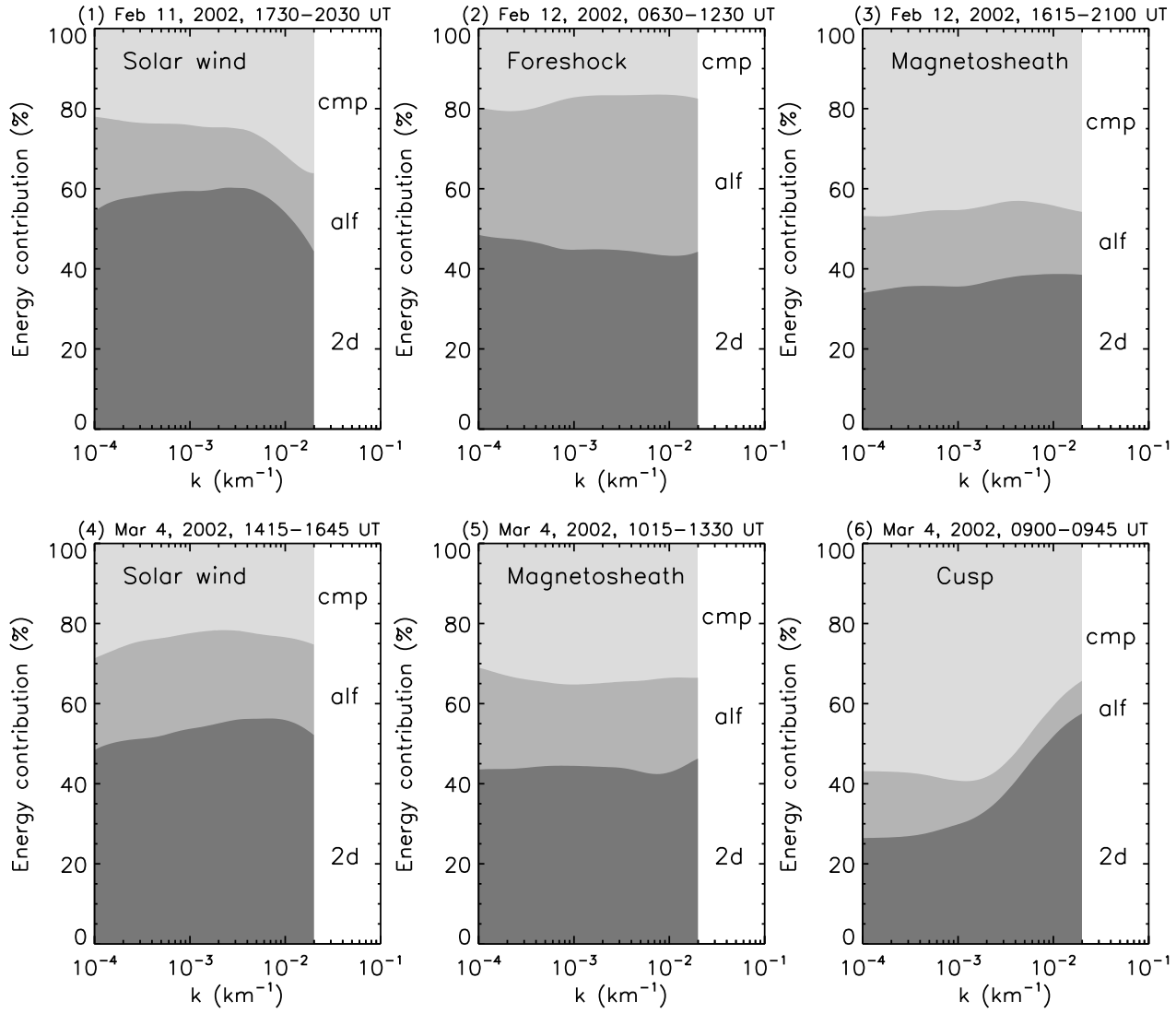

Figure 7. Energy contribution of the three fluctuation components in various regions.

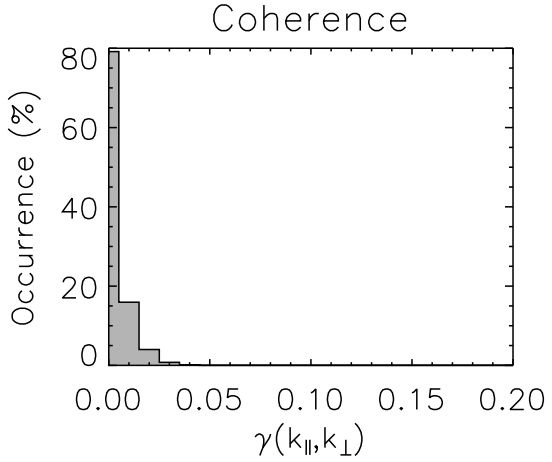

Figure 8. Histogram of coherence between the two-dimensional and the Alfvénic component.